Received: 5 May 2021 | Revised: 22 October 2021 | Accepted: 25 October 2021
DOI: 10.1002/joc.7432

RESEARCH ARTICLE

International Journal of Climatology RMetS

# Influence of Okhotsk Sea blocking on summer precipitation over South Korea

**Chan-Yeong Song**[1] | **Joong-Bae Ahn**[2]

[1]Department of Atmospheric Sciences, BK21 School of Earth and Environmental Systems, Pusan National University, Busan, South Korea

[2]Department of Atmospheric Sciences, Pusan National University, Busan, South Korea

**Correspondence**
Joong-Bae Ahn, Department of Atmospheric Sciences, Pusan National University, 2, Busandaehak-ro 63beon-gil, Geumjeong-gu, Busan 46241, Souh Korea.
Email: jbahn@pusan.ac.kr

**Funding information**
Korea Meteorological Administration Research and Development, Grant/Award Number, Grant/Award Number: KMI2020-01411.

**Abstract**

This study examined the influence of atmospheric blocking on the variability of precipitation over South Korea during summer (June–July–August) by defining the blocking frequency over the Okhotsk Sea (Okhotsk Sea blocking frequency; OK_BF). According to composite analysis for the years of high precipitation over South Korea, blocking occurs more frequently over the Okhotsk Sea (140°E–160°E). Partial correlation and regression analyses were conducted to separate the contribution of OK_BF to precipitation variability from that of the low-level meridional wind (LLMW) because LLMW over the region is another important aspect of summer precipitation in South Korea. The barotropic structures of positive geopotential height anomalies over the Okhotsk Sea associated with increasing OK_BF can induce negative temperature anomalies over South Korea due mainly to the equatorward advection of cold air masses from higher latitudes. The enhanced meridional temperature gradient can cause increases in baroclinic instability and zonal wind vertical shear according to the thermal wind balance. This instability can induce anomalous cyclonic circulations over South Korea, resulting in positive precipitation anomalies. The partial correlation coefficients ($R^2 = 0.35$–$0.40$) between the OK_BF and precipitation indices, including mean precipitation, extreme precipitation intensity, wet days, and consecutive wet days, were all statistically significant at the 95% confidence level. Overall, the effects of the increasing OK_BF on both precipitation and potential evapotranspiration can intensify the surface water budget in South Korea.

**KEYWORDS**

blocking, Okhotsk Sea, potential evapotranspiration, precipitation, South Korea

## 1 | INTRODUCTION

A significant portion of precipitation over South Korea is concentrated during summer (June–July–August). The summer climate in East Asia, including Korea, Japan, and China, is closely related to the East Asian Summer Monsoon (EASM), which consists of many subsystems, including Baiu in Japan, Changma in Korea, and Meiyu in China (BCM, for example, Hong and Ahn, 2015). Therefore, the variability of summer precipitation in

South Korea has generally been conducted in the frame of EASM (e.g., Ha *et al.*, 2012; Lee and Seo, 2013; Park *et al.*, 2015). The intensity of the EASM is generally modulated by the variability of the western North Pacific subtropical high (WNPSH). According to Chang *et al.* (2000a, 2000b), the enhanced low-level jet associated with the westward extension of the WNPSH provides higher moisture transport into East Asia, resulting in increased precipitation over the region. On the other hand, unlike other monsoon systems in the tropics–subtropics, the EASM is a subtropical–mid-latitude synoptic-scale circulation system. The combined influences from mid- and low-latitudes complicate the understanding of the EASM (Wang *et al.*, 2008; Ha *et al.*, 2012). Therefore, many researchers have investigated the relationship between interannual variability of the EASM and various factors, such as El Niño–Southern Oscillation (e.g., Wang *et al.*, 2000; Yun *et al.*, 2010; Wu *et al.*, 2012; Kim and Kug, 2018), Arctic Oscillation (e.g., Gong and Ho, 2003; Gong *et al.*, 2011), North Atlantic Oscillation (NAO) or North Atlantic sea surface temperature (NASST) (e.g., Wu *et al.*, 2009, 2012; Zuo *et al.*, 2013; Zheng *et al.*, 2016), and tropical Atlantic sea surface temperature (TASST) (e.g., Ham *et al.*, 2017; Choi and Ahn, 2019).

Blocking is a synoptic-scale quasistationary atmospheric phenomenon that is associated with the formation of strong stationary anticyclones at high latitudes, resulting in weakening (strengthening) zonal (meridional) circulation (Rex, 1950a, 1950b). This synoptic phenomenon is usually related to extreme weather events, such as coldwaves (Buehler *et al.*, 2011), heatwaves (Barriopedro *et al.*, 2011), heavy rain (Grams *et al.*, 2014), and drought (García-Herrera *et al.*, 2007), depending on where the blocking is located. Although the frequency and intensity of the summer blocking activities are lower than in winter, the specific role of those systems on the mid-latitude climate has been studied widely. Sousa *et al.* (2017) reported that the south of the blocked regions (the region of the blocks) exhibits positive (negative) precipitation anomalies. A dipole in the precipitation anomalies under blocking action was confirmed for many regions, including Europe (Sousa *et al.*, 2016) and South America (Rodrigues and Woollings, 2017; Fernandes and Rodrigues, 2018). These studies suggested that the blocking phenomenon is associated directly with the variability of precipitation.

The formation and maintenance of blocking anticyclones are not completely understood because of their nonlinear characteristics, such as internal dynamics, orographic effects, and baroclinic transient eddies (Shutts, 1983; Mullen, 1987; Nakamura and Wallace, 1993; Nakamura and Fukamachi, 2004). Nevertheless, considerable efforts have been made to understand summer blocking. Previous studies reported the relationship between summer blocking and land-sea thermal contrast. Arai and Kimoto (2005) showed that increased meridional surface temperature gradient between the Arctic Sea and Eurasia enhances the polar frontal jet, which is a waveguide of quasi-stationary Rossby waves. Nakamura and Fukamachi (2004) suggested that Rossby wave breaking leads to blocking formation over the Sea of Okhotsk (hereafter, Okhotsk Sea). Several studies reported that the positive phase of summer Northern Hemisphere annular mode could account for much of the anomalous weather associated with the double jet stream structure (polar and subtropical jet streams) and blocking high (Ogi *et al.*, 2005; Tachibana *et al.*, 2010). He *et al.* (2018) reported that the land-sea thermal contrast and summer blocking form positive feedback, and both show an increasing trend. They suggested that the land-sea thermal forcing can induce a zonal-mean westerly and double jet stream, which are favourable conditions for more frequent blocking.

The Okhotsk high (OKH) is a cold high near the surface that is generally accompanied by a blocking anticyclone in the middle and upper troposphere. The occurrence of the OKH brings cool and wet air masses to East Asia (e.g., Ninomiya and Mizuno, 1985). According to Nakamura and Fukamachi (2004), the formation of the OKH in July is related to the eastward propagation of a quasi-stationary Rossby wave. Many studies reported that the anomalous OKH is related to the Atlantic–Europe–Asia (AEA) teleconnection pattern (e.g., Wu *et al.*, 2009, 2012; Zuo *et al.*, 2012, 2013; Zheng *et al.*, 2016). These teleconnection patterns start mainly from the subtropical North Atlantic and propagate eastward to North Europe, the Urals, Central Eurasia, and the Okhotsk Sea. The AEA teleconnection pattern has been associated with the NAO, NASST, and TASST (Zuo *et al.*, 2012, 2013; Zheng *et al.*, 2016; Choi and Ahn, 2019). Meanwhile, some studies emphasized that the Pacific-Japan (PJ) or East Asia-Pacific (EAP) teleconnection patterns, which have a meridional tripole structure consisting of WNPSH, BCM front, and OKH, are closely related to summer precipitation in East Asia (Chen and Zhai, 2015; Wang *et al.*, 2018). According to previous studies, convective heating in the western North Pacific can induce an anomalous cyclone (anticyclone) over East Asia (Okhotsk Sea) by generating a meridional teleconnection pattern (Nitta, 1987; Yim *et al.*, 2008).

The blocking anticyclone appearing in the Okhotsk Sea (Hereafter, Okhotsk Sea blocking, OKB) can also play an important role in influencing the EASM. Park and Ahn (2014) reported that summertime (June–July–August) blocking is the primary mode in the Okhotsk Sea according to principal component analysis using the 500 hPa geopotential heights. They showed that the OKB frequencies have a distinct negative (positive) correlation with summer temperature (precipitation) in East Asia. Their results suggest that the characteristics of the summer climate over East Asia are closely associated with the occurrence of the OKB. On the other hand, most studies focused on the relationship between the OKB and precipitation over East Asia and specific regions (Japan and China), rather than just South Korea (Wang, 1992; Nakamura and Fukamachi, 2004; Park and Ahn, 2014; Chen and Zhai, 2014b).

Precipitation deficits have a direct impact on the occurrence of drought, which causes significant damage to various aspects of agriculture, society, and the economy. According to previous studies, extreme droughts in South Korea occurred in 1927–1930, 1938–1945, 1951–1952, 1967–1969, 1994–1996, and 2013–2015, caused mainly by successive shortages of summer rainfall for multiple years (Kim *et al*., 2011; Zhang and Zhou, 2015; Kwon *et al*., 2016). In an attempt to understand drought in South Korea better, many studies have investigated the characteristics, such as spatiotemporal variation (Min *et al*., 2003; Azam *et al*., 2018; Kwon *et al*., 2019), the relationship with preceding climate conditions (Choi *et al*., 2009, 2011), and future projection (Im *et al*., 2012; Choi *et al*., 2016; Lee *et al*., 2019). Furthermore, potential evapotranspiration (PET), as a function of temperature, is another climate factor impacting drought conditions (Easterling *et al*., 2007; Im *et al*., 2012). Therefore, it is necessary to study the effects of blocking on water budget components, including precipitation and PET, which can help understand the flood and drought mechanisms over this region. Focusing on South Korea and the vicinity, this study examined the detailed relationship between the OKB frequencies and both precipitation and PET in the region.

As mentioned earlier, the EASM is closely related to warm and moist air advection at the low-level from the low-latitude regions to the mid-latitude regions. These are favourable conditions for the generation of convective instability. In contrast, the atmospheric blocking activities are accompanied by baroclinic instability (Wang, 1992; Nakamura and Fukamachi, 2004). Therefore, the role of OKB on baroclinic instability is discussed by separating it from convective instability.

Based on the above issues, this paper is organized as follows. Section 2 describes the data, definition of the indices, and statistical method. Section 3 describes the influence of the occurrence of OKB on the water budget components, including precipitation and PET, over South Korea. A discussion and summary are given in Sections 4 and 5, respectively.

## 2 | DATA AND METHOD

### 2.1 | Data

The data used in this study were the monthly mean enhanced precipitation reanalysis data provided by the Climate Prediction Center Merged Analysis of Precipitation (CMAP) with a horizontal resolution of $2.5° \times 2.5°$ (Xie and Arkin, 1997). The daily and monthly mean atmospheric fields were obtained from the National Centers for Environmental Prediction (NCEP) Department of Energy Reanalysis 2 dataset (hereafter, NCEP2) with a horizontal resolution of $2.5° \times 2.5°$ (but $1.875° \times 1.875°$ for 10-m horizontal wind) (Kanamitsu *et al*., 2002). The monthly mean temperature and precipitation data from 60 in-situ stations of the Korea Meteorological Administration were also used to support the results derived from the reanalysis data. The period analysed in this study was from 1979 to 2020. Figure 1a represents the topography and location of weather observation stations over South Korea. The topography data used in this study were ASTER Global Digital Elevation Model Version 3 (ASTGTM) (Abrams *et al*., 2020). The CMAP precipitation data were interpolated onto an NCEP2 grid point to facilitate a comparison with the NCEP2 data. The variability of CMAP precipitation was highly consistent with that of the precipitation averaged over 60 weather stations located in South Korea (Figure 1b). The northeastern Asian summer monsoon index (NEASMI) was defined by the U850 (25°N–35°N, 110°E–150°E) (NEASM_SI) minus U850 (45°N–55°N, 110°E–150°E) (NEASM_NI), where U850 represents the zonal wind at 850 hPa (Park *et al*., 2018).

### 2.2 | Definition of the Eady growth rate

The Eady growth rate (Eady, 1949; Lindzen and Farrell, 1980; Hoskins and Valdes, 1990) was used to measure the baroclinic instability. This parameter is related directly to the vertical wind shear (or meridional thermal gradient due to thermal wind balance) and static stability. The maximum Eady growth rate is defined as follows:

$$\sigma = 0.31 \frac{f}{N} \left| \frac{\partial u}{\partial Z} \right|,$$

where $f$ is the Coriolis parameter, $N$ is the Brunt–Väisälä frequency, $u$ is the horizontal wind vector, and $z$ is the vertical height.

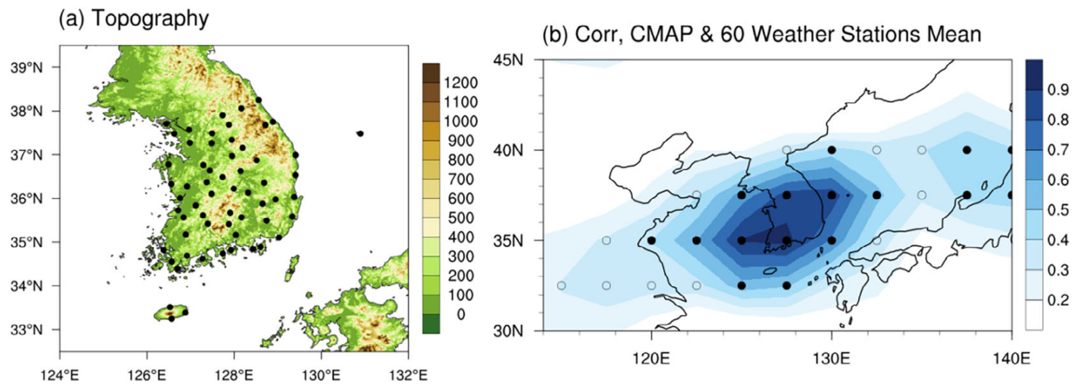


FIGURE 1 (a) Topography (shading; unit: m) and location of the observation stations (black dots) over South Korea. (b) Correlation maps between two precipitation datasets during the period of 1979–2020 (JJA); one is CMAP precipitation, and another is precipitation averaged over 60 weather stations located in South Korea. The opened (closed) circles in (b) indicate that the correlation coefficients are significant at the 95% (99%) confidence level [Colour figure can be viewed at wileyonlinelibrary.com]

## 2.3 | Definition of the PET

The surplus and deficit are the basic concepts of the water balance equation. Based on this concept, the standardized precipitation evapotranspiration index (Vicente-Serrano *et al.*, 2010), which was comprised of precipitation and PET, is a widely used index to identify drought conditions over South Korea (Kim *et al.*, 2012, 2013; Sohn *et al.*, 2013; Nam *et al.*, 2015). The monthly PET was calculated using the method proposed by Thornthwaite (1948):

$$\mathrm{PET} = 16K\left(\frac{10T}{\mathrm{I}}\right)^{\mathrm{m}},$$

where PET is in $\mathrm{mm \cdot month^{-1}}$, and $T$ is the monthly mean air temperature (°C). $K$ is the correction coefficient calculated as a function of the latitude and month (Vicente-Serrano *et al.*, 2010):

$$K = \left(\frac{N}{12}\right)\left(\frac{\mathrm{NDM}}{30}\right),$$

where NDM is the number of days in the month. $N$ is the maximum sunshine duration in hours and was calculated as follows:

$$N = \left(\frac{24}{\pi}\right)\omega_{\mathrm{S}},$$

$$\omega_{\mathrm{S}} = \arccos(-\tan\varphi\tan\delta),$$

$$\delta = 0.4093\sin\left(\frac{2\pi J}{365} - 1.405\right),$$

where $\omega_{\mathrm{S}}$ is the hourly angle of the sun rising; $\varphi$ is the latitude; $\delta$ is the solar declination; $J$ is the average Julian day of the month.

$I$ is the heat index, which was calculated from the monthly heat index ($i_j$):

$$I = \sum_{\mathrm{j}=1}^{12} i_j, \text{where } i_j = \left(\frac{T_j}{5}\right)^{1.514}$$

$m$ is a constant that given by a third-order polynomial with respect to $I$:

$$m = 6.75\times10^{-7}\mathrm{I}^3 - 7.71\times10^{-5}\mathrm{I}^2 + 1.79\times10^{-2}\mathrm{I} + 0.4924$$

## 2.4 | Definition of the blocking index

The blocking events were defined according to Barriopedro *et al.* (2006). This index, which is based on the index proposed by Tibaldi and Molteni (1990), was used most widely in previous studies (You and Ahn, 2012; Park and Ahn, 2014; Choi and Ahn, 2017; Lee and Ahn, 2017). The northern and southern 500 hPa geopotential height gradient (GHGN and GHGS, respectively) were calculated at each longitude as follows:

$$\mathrm{GHGN}(\lambda) = \frac{\mathrm{Z}(\lambda, \phi_{\mathrm{N}}) - \mathrm{Z}(\lambda, \phi_0)}{\phi_{\mathrm{N}} - \phi_0}$$

$$\mathrm{GHGS}(\lambda) = \frac{\mathrm{Z}(\lambda, \phi_0) - \mathrm{Z}(\lambda, \phi_{\mathrm{S}})}{\phi_0 - \phi_{\mathrm{S}}}$$

$$\phi_{\mathrm{N}} = 77.5^\circ\mathrm{N} + \Delta$$

$$\phi_0 = 60.0°\mathrm{N} + \Delta$$

$$\phi_S = 40.0°\mathrm{N} + \Delta$$

where $\Delta = -5.0°, -2.5°, 0.0°, 2.5°$, or $5.0°$.

$Z(\lambda,\phi)$ is the 500 hPa geopotential height at longitude ($\lambda$) and latitude ($\phi$). As the five different latitudes were applied, the respective five results of GHGN($\lambda$) and GHGS($\lambda$) were obtained. A given longitude was considered to be blocked when both GHGN($\lambda$) and GHGS($\lambda$) satisfied the following condition in at least one of the five different latitudes.

$$\mathrm{GHGN}(\lambda) < -10\,\mathrm{m}\,(°\mathrm{latitude})^{-1} \text{ and } \mathrm{GHGS}(\lambda) > 0\,\mathrm{m}\,(°\mathrm{latitude})^{-1}$$

One persistent blocking event of each longitude was defined as occurring when these conditions lasted for at least five consecutive days. The blocking frequency (BF) was defined as the ratio of the days in which persistent blocking events occur (i.e., blocking days) to the total number of days in summer (92 days).

Because blocking exhibits a significant longitudinal extension, previous efforts to quantify blocking frequency have commonly applied an extension criterion. For example, Barriopedro *et al.* (2006) applied the following:

1. At least five consecutive blocked longitudes (12.5°)
2. A nonblocked longitude between the two blocked longitudes is considered a blocked longitude.

However, we did not apply the above extension criterion to the blocking definition for two reasons. First, the BFs decreased when the extension criterion was applied (Figure S1a). Second, application of the extension criterion had little impact on the interannual variability in blocking frequency, particularly in regions of prominent blocking activity (Figure S1b).

### 2.5 | Statistical analysis

This study utilized several statistical analyses, including composite, correlation (or equivalently regression), and partial correlation (regression) analysis, to examine the relationship between the OKB frequencies and precipitation over South Korea. The correlation method applied was the linear Pearson correlation ($R$). The independent associations between the above-mentioned two phenomena were quantified using partial correlation analysis. Partial correlation calculates the correlation between the two variables while eliminating the influence of another variable. Many studies have selected the same analysis to distinguish the impact of one factor from that of the other (e.g., As-syakur *et al.*, 2014; He and Zhu, 2015; Choi and Ahn, 2019). The partial correlation coefficient $R_{xy,z}$ between variable $x$ and $y$ without the effect from z was calculated as:

$$R_{xy,z} = \frac{R_{xy} - R_{xz}R_{yz}}{\sqrt{(1 - R_{xz}{}^2)(1 - R_{yz}{}^2)}},$$

where $R_{xy}$, $R_{xz}$, and $R_{yz}$ represent the correlation coefficients between $x$ and $y$, $x$ and $z$, and $y$ and $z$, respectively. The two-sided Student's $t$ test, a parametric test, and Mann–Whitney $U$ test (Mann and Whitney, 1947), a nonparametric test, were used to assess the statistical significance of the differences between two composites (null hypothesis of equal means). The two-sided Student's $t$ test was used to evaluate the confidence level of the correlation (null hypothesis is that the two variables are independent). In this paper, $p$ values <.05 were considered statistically significant.

## 3 | RESULT

### 3.1 | Blocking regions associated with summer precipitation over South Korea

Figure 2 represents the climatological summertime BF over the Northern Hemisphere along the longitude. The four major regions with high BFs were found in Northern Europe (NE, 0°E–50°E), Ural region (UR, 50°E–80°E), Okhotsk Sea (OK, 120°E–160°E), and Northeastern Pacific (NP, 160°W–130°W). This result is consistent with that reported elsewhere (e.g., Park and Ahn, 2014; Antokhina *et al.*, 2016).

Composite analysis was conducted to specify the blocking regions associated with precipitation over South Korea (Figure 3). The PREC_SK was defined by averaging the precipitation obtained from 60 in-situ stations. The high (low) PREC_SK years were defined as values higher (lower) than 1 SD of the time series from 1979 to 2020 (Table 1). The BFs over the region of the UR (50°E–70°E) and OK (140°E–160°E) were higher during the high PREC_SK years than during the low PREC_SK years. In the present study, the UR_BF (OK_BF) was defined as the area-averaged BFs over the region of 50°E–70°E (140°E–160°E). The composite difference of UR_BF was 2.36%, which is not significant at the 95% confidence level (from two-sided Student's $t$ test and Mann–Whitney $U$ test, the $p$ values were .18 and .16, respectively). The composite difference of OK_BF was 5.66%, which is significant at the 95% confidence level

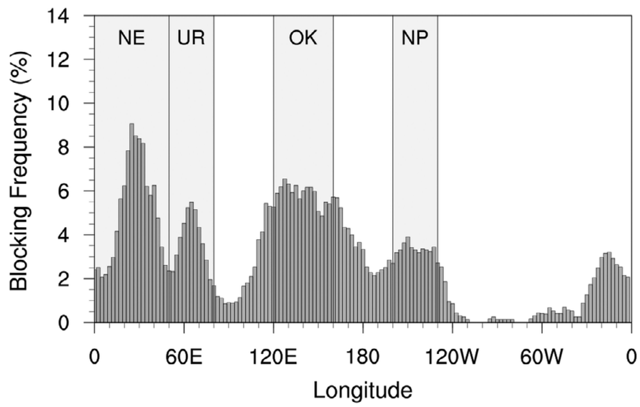


**FIGURE 2** Climatology of the blocking frequency in June–July–August (JJA) for the period of 1979–2020

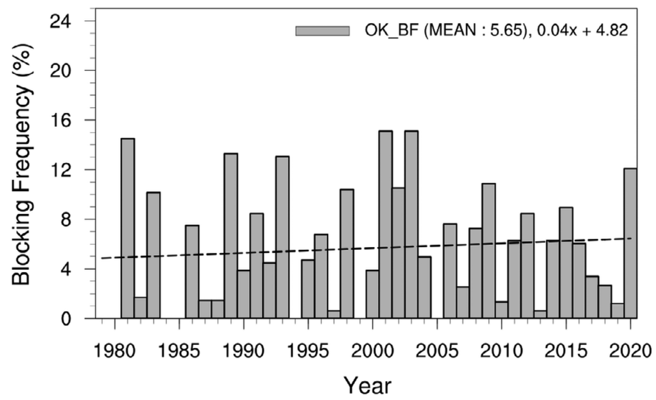


**FIGURE 4** Time series of OK_BF for 1979–2020 (JJA). The dashed line indicates the linear regression line, as described by the equation in the figure

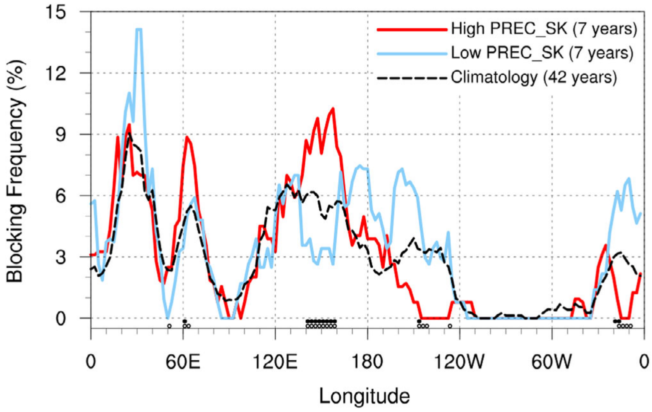


**FIGURE 3** Composite of the blocking frequency for high and low PREC_SK years based on the ±1 SD of the total time series (1979–2020). The dashed line denotes that the climatological values. The closed (opened) circles indicate the longitudes where the composite differences of the blocking frequency are significant at the 90% confidence level with a two-sided Student's *t* test (Mann–Whitney *U* test) [Colour figure can be viewed at wileyonlinelibrary.com]

**TABLE 1** Classification of the high and low PREC_SK years based on the ±1 SD

| High PREC_SK years (+1 SD) | Low PREC_SK years (−1 SD) |
|---|---|
| 1987, 1998, 2002, 2003, 2006, 2011, 2020 | 1982, 1988, 1992, 1994, 2015, 2016, 2019 |

(from two-sided Student's *t* test and Mann–Whitney *U* test, the *p* values were .02 and .03, respectively). These results are in line with previous studies reporting that persistent extreme precipitation in Central-Eastern China is closely associated with double-blocking high patterns, which have positive geopotential height anomaly around the Ural Mountains and around the Okhotsk Sea (Chen and Zhai, 2014a, 2014b). As mentioned in the introduction, a stationary Rossby wave train from northern Europe can induce the development of a Ural high and OKH. The direct effects of blocking on precipitation over South Korea were examined by focusing only on the blocking events in the Okhotsk Sea. This study focused on the relationship between the OK_BF and precipitation in South Korea over interannual timescales. The evolution mechanism of OKB is beyond our scope and this issue will be discussed in more detail in the discussion.

### 3.2 | The interannual variation of OK_BF and its association with precipitation over South Korea

Figure 4 presents the time series of OK_BF. The climatological value of OK_BF was 5.65%. The OK_BF exhibited a long-term trend embedded in the interannual variation. The linear trend was 0.04% year$^{-1}$, which is not significant at the 95% confidence level. These results agree with He *et al.* (2018). They reported that summer blocking increases with increasing summer land-sea thermal contrast, representing the zonal asymmetric thermal forcing changes under global warming.

Composite analysis for the high and low PREC_SK years was also conducted separately to examine the effect of the duration of OK_BF (Figure 5). The composite differences of OK_BF for five duration groups (i.e., 5, 6, 7, 8, and more than 9 days) were 0.26, 1.24, 1.57, 0.55, and 2.04%, respectively. The BFs were all higher during the high PREC_SK years than during the low PREC_SK years, regardless of the duration, but these are not significant at the 95% confidence level based on both two-sided

Student's $t$ test and Mann–Whitney $U$ test. This insignificant difference might be due to the low OK_BF value according to the duration (i.e., few blocking events), indicating that further analysis, such as identical analysis using long-term data or case study, is required.

Correlation analysis was conducted to examine the relationship between OK_BF and precipitation over South Korea during summer. The PREC_NEA was defined by the area averaging the precipitation over northeastern Asia (NEA; 30°N–50°N, 110°E–145°E) (Lee *et al.*, 2005). The correlation coefficient between OK_BF and PREC_NEA was 0.40, which is significant at the 95% confidence level. Similarly, NEASM_NI, which is the northern component of NEASMI, was closely related to OK_BF with correlations of −0.41, which is significant at the 99% confidence level (the correlation coefficients between OK_BF and NEASMI and between OK_BF and NEASM_SI were 0.28 and 0.14, respectively). On the other hand, OK_BF was not significantly correlated with precipitation over South Korea (Figure S2a). This result was also revealed by analysing the in-situ precipitation data. The correlation coefficient between OK_BF and station-averaged precipitation (i.e., PREC_SK) was only 0.27, which is insignificant at the 95% confidence level. Nevertheless, significant positive correlations were observed at 10 stations (Figure S2b). These results agree with those obtained by Park and Ahn (2014), who reported a low correlation coefficient of 0.15 between OK_BF and PREC_SK (figure 3 and table 6 in Park and Ahn, 2014). They attributed this insignificant relationship to the locality of precipitation over South Korea. The above results suggest that OK_BF is associated with the precipitation over South Korea, but it is unclear if this relationship is robust and how OK_BF contributes to precipitation variability because of their low correlation coefficients in most regions.

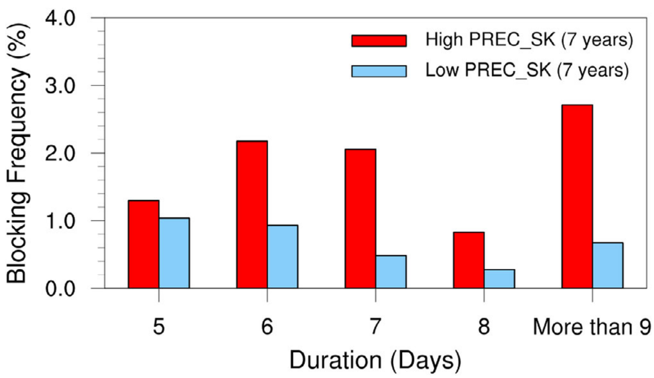


**FIGURE 5** Distribution of the OK_BF along with the duration (≥5 days) for high and low PREC_SK years [Colour figure can be viewed at wileyonlinelibrary.com]

We conjectured that other factors strongly modulated the variability of precipitation over South Korea, which are distinct from OK_BF. Figure 6a shows the long-term (1979–2020, JJA) means of the meridional wind in the lower troposphere (850 hPa) and geopotential height in the middle troposphere (500 hPa). In summer, the high-pressure system is located in the subtropical western North Pacific (so-called WNPSH). The poleward wind is dominant in East Asia, which is located on the western flank of the WNPSH (5,880 m isoline in Figure 6a). As mentioned in the introduction, the moisture transported from low latitudes to East Asia is a general consensus on the critical role of the EASM. In line with this issue, many studies on Korean summer precipitation focused on the impact of northward moisture transport across the southern boundaries of South Korea (e.g., Hwang and Lee, 1993; Ha *et al.*, 2003; Park *et al.*, 2003; Shin and Lee, 2005; Baek *et al.*, 2017; Kim *et al.*, 2017). Although a nonlinear relationship between the WNPSH and precipitation over South Korea was reported

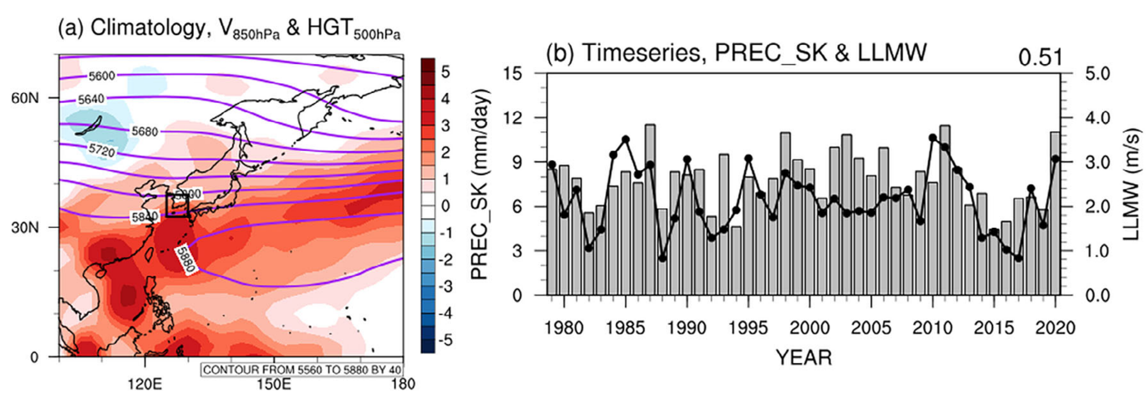


**FIGURE 6** (a) Climatology of 850-hPa meridional wind (shading; unit: $m \cdot s^{-1}$) and 500-hPa geopotential height (contour; unit: m) during 1979–2020 (JJA). The black-line box indicates the domain (32.5°N–37.5°N, 125°E–130°E) of the LLMW defined in this study. (b) Time series of the PREC_SK (bars with left-hand scale) and LLMW (line with right-hand scale). PREC_SK is defined by averaging the precipitation obtained from 60 in-situ stations. The value of the upper-right corner above (b) indicates the correlation coefficient between PREC_SK and LLMW [Colour figure can be viewed at wileyonlinelibrary.com]

(Yeo *et al.*, 2020), the link between the southerly wind and precipitation over South Korea is evident (figure 3 in Yeo *et al.*, 2020). Low-level meridional wind (LLMW) over South Korea has a significant positive correlation with the PREC_SK, which is significant at the 99% confidence level (Figure 6b). The LLMW index was defined by area averaging the 850-hPa meridional wind over South Korea (32.5°N–37.5°N, 125°E–130°E). The correlation coefficient between the OK_BF and LLMW was −0.13, indicating that both variations are almost independent statistically. These results confirmed that both variations were related to the precipitation variability over South Korea with different mechanisms. Thus, partial correlation and regression analyses were performed to separate the contribution of the OK_BF to precipitation variability from that of the LLMW.

## 3.3 | Influence of frequent occurrence of OKB on precipitation and potential evapotranspiration over South Korea

Figure 7 presents the partial regression maps of geopotential height anomalies onto the normalized OK_BF after excluding the effects of the LLMW. Pronounced

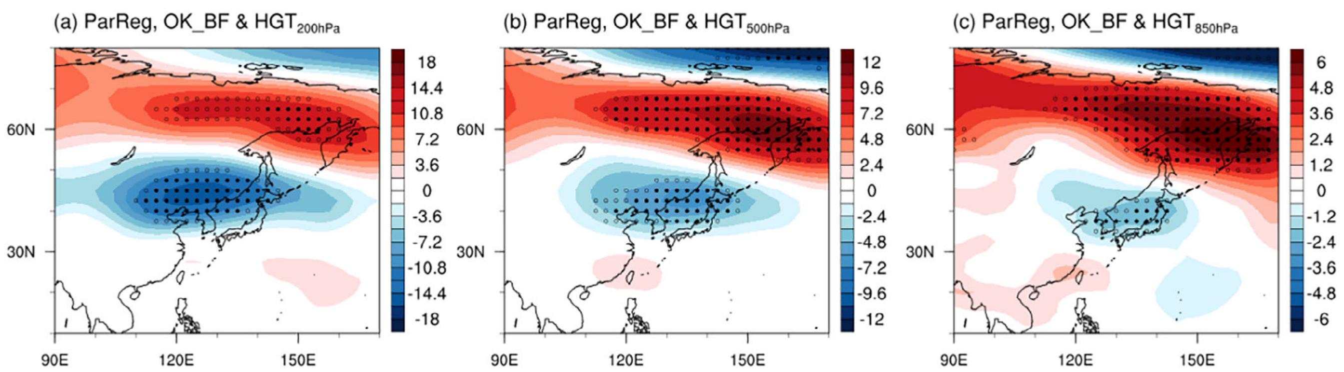


**FIGURE 7** Partial regression maps of the (a) 200 hPa, (b) 500 hPa, and (c) 850 hPa geopotential height anomalies (unit: m) onto the normalized OK_BF after excluding the effects of the LLMW. The opened (closed) circles indicate that the correlation coefficients are significant at the 90% (95%) confidence level [Colour figure can be viewed at wileyonlinelibrary.com]

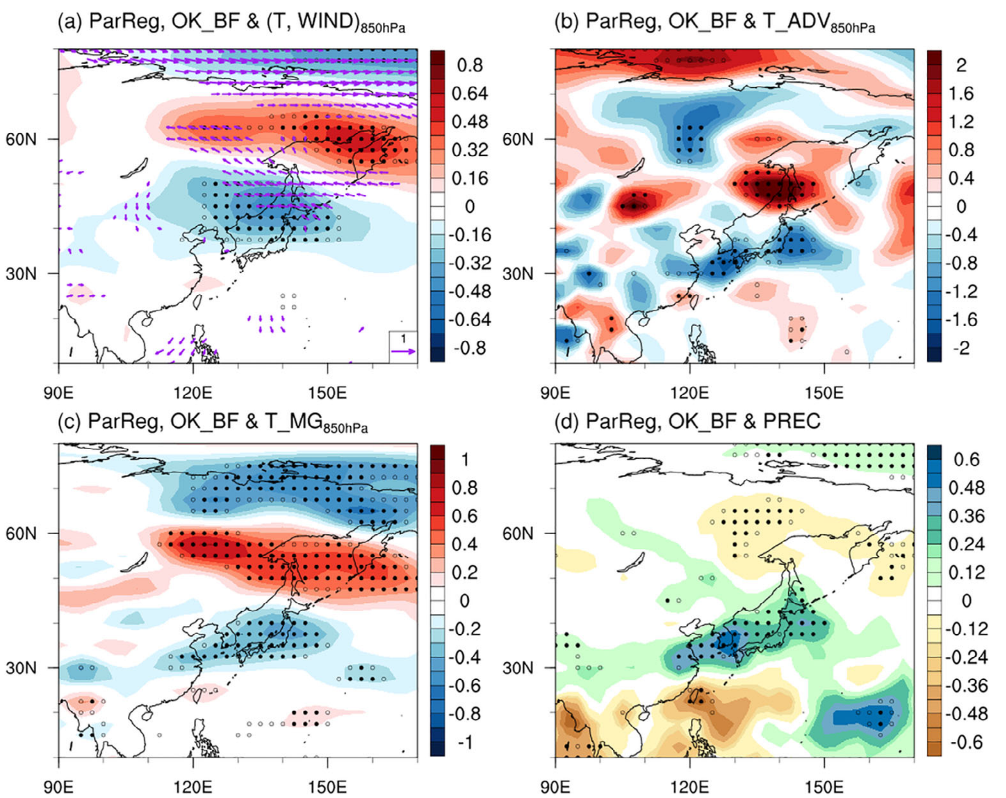


**FIGURE 8** Partial regression maps of the (a) 850 hPa air temperature (shading; unit: K), horizontal wind (vectors; unit: $m \cdot s^{-1}$), (b) temperature advection (shading; unit: $deg \cdot s^{-1} \times 10^{-6}$), (c) meridional temperature gradient (shading; unit: $deg \cdot m^{-1} \times 10^{-6}$), and (d) precipitation (shading; unit: $mm \cdot day^{-1}$) anomalies onto the normalized OK_BF after excluding the effects of the LLMW. The opened (closed) circles indicate that the correlation coefficients are significant at the 90% (95%) confidence level. Only the vectors in (a) statistically significant at the 90% confidence level are shown [Colour figure can be viewed at wileyonlinelibrary.com]

barotropic positive geopotential height anomalies were observed over the Okhotsk Sea (Figure 7a–c). Blocking is often associated with a high-pressure system on the poleward side and low-pressure systems on the equatorward side (Barriopedro *et al.*, 2006), which exhibits a significant meridional component. Negative geopotential height anomalies over South Korea were evident from the lower to upper troposphere because the trough axis crosses Korean Peninsula (Figure 7a–c). The anomalous anticyclone over the Okhotsk Sea can help maintain the anomalous cyclone over South Korea. Partial regression analyses of air temperature, horizontal temperature advection, and meridional temperature gradient in the lower troposphere (850 hPa) were also conducted to obtain evidence to support this hypothesis (Figure 8a–c). The negative temperature anomalies were confirmed over regions, including Korean Peninsula and Japan (Figure 8a). This is due mainly to the equatorward advection of cold air masses from higher latitudes (Figure 8a, b). In particular, the enhanced meridional temperature gradient, which is one of components of the horizontal temperature advection, was clearly confirmed over the regions mentioned above (Figure 8c). At the same regions, significant positive precipitation anomalies were clearly evident (Figure 8d). The temperature advection of cold air, which is associated with the enhanced meridional temperature gradient, can accelerate the upward motion by the strengthened baroclinic instability. These relationships are discussed in more detail below.

The vertical structure of air temperature, meridional temperature gradient, and vertical and zonal winds near South Korea associated with increasing OK_BF were

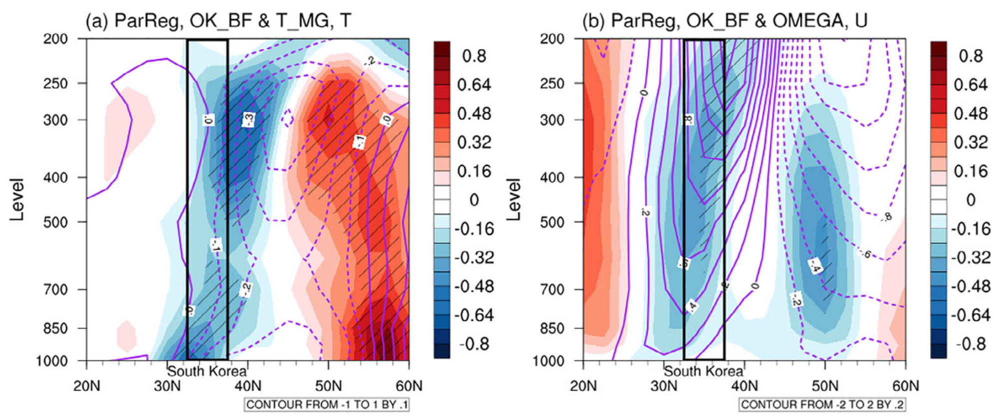


**FIGURE 9** Meridional–vertical cross-section averaged along 125°E–130°E for (a) meridional temperature gradient (shading; unit: $\mathrm{deg \cdot m^{-1} \times 10^{-6}}$), air temperature (contour; unit: K), (b) omega (shading; unit: $\mathrm{Pa \cdot s^{-1} \times 10^{-2}}$) and zonal wind (contour; unit: $\mathrm{m \cdot s^{-1}}$) anomalies partially regressed upon the normalized OK_BF after excluding the effects of the LLMW. Hatching indicates that the correlation coefficients are significant at the 95% confidence level. The black-line boxes indicate the location of South Korea (32.5°N–37.5°N) [Colour figure can be viewed at wileyonlinelibrary.com]

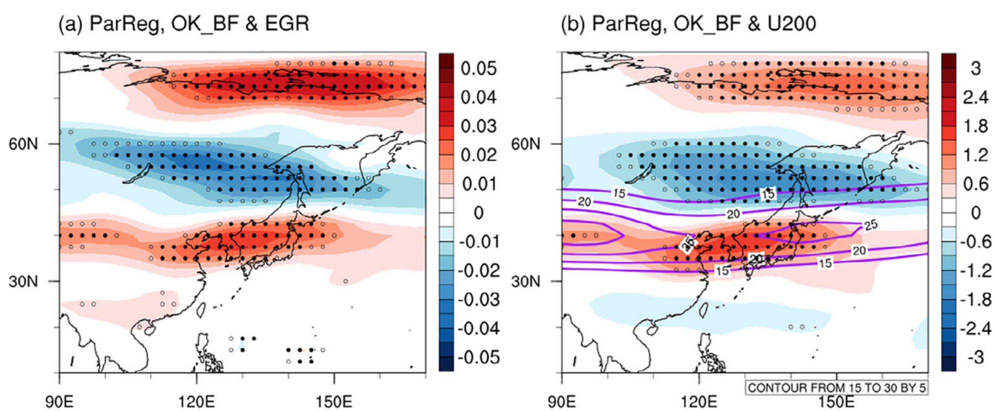


**FIGURE 10** Partial regression maps of the (a) vertically averaged maximum Eady growth rate between 200 and 850 hPa (unit: $\mathrm{day^{-1}}$) and (b) 200 hPa zonal wind (unit: $\mathrm{m \cdot s^{-1}}$) anomalies onto the normalized OK_BF after excluding the effects of the LLMW. The opened (closed) circles indicate that the correlation coefficients are significant at the 90% (95%) confidence level. The contour in (b) indicates the climatological 200 hPa zonal wind [Colour figure can be viewed at wileyonlinelibrary.com]

examined further (Figure 9). The vertically uniform negative (positive) temperature anomalies were confirmed at the northern regions of South Korea (between 35°N and 55°N), indicating the enhanced meridional temperature gradient over South Korea (Figure 9a). The enhanced meridional temperature gradient can induce baroclinic instability, leading to anomalous cyclonic circulations and ascending motion. This enhanced meridional temperature gradient strengthens the zonal wind vertical shear according to the thermal wind balance (Figure 9b). These results correspond to the increased baroclinicity near the 40°N latitude (Figure 10a). The strong upper-level subtropical jet is generally located along the belt of 40°N latitude. This subtropical jet was strengthened further by the reinforced meridional temperature gradient induced by the blocking anticyclone. The positive (negative) zonal wind anomalies around latitude 75°N (55°N) were formed directly by the blocking anticyclone. Overall, the enhanced double jet stream, which has a positive zonal wind anomalies around the polar (approximately 75°N) and subtropical (approximately 40°N) jet streams, was present (Figure 10b). As mentioned in previous studies (Ogi *et al.*, 2005; He *et al.*, 2018), the enhanced double jet structure may inversely lead to a more frequent

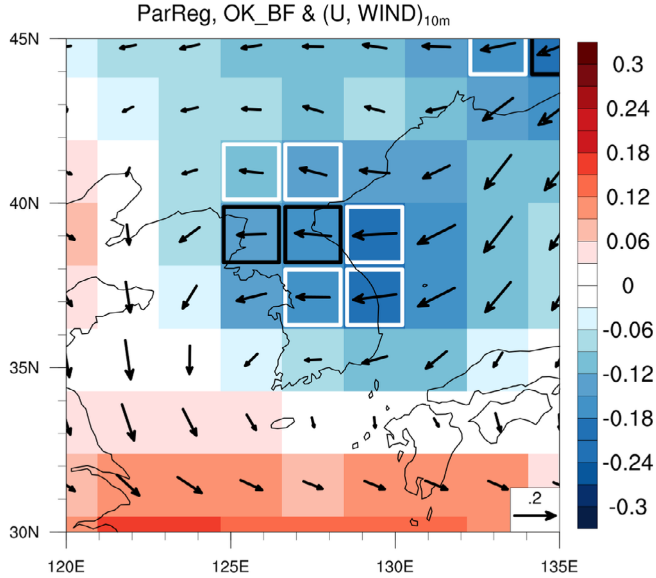


**FIGURE 12** Partial regression maps of the 10-m zonal (shading; unit: $m \cdot s^{-1}$) and horizontal wind (vector, unit: $m \cdot s^{-1}$) anomalies onto the normalized OK_BF after excluding the effects of the LLMW. The white (black)-line boxes indicate that the correlation coefficients of zonal wind are significant at the 90% (95%) confidence level [Colour figure can be viewed at wileyonlinelibrary.com]

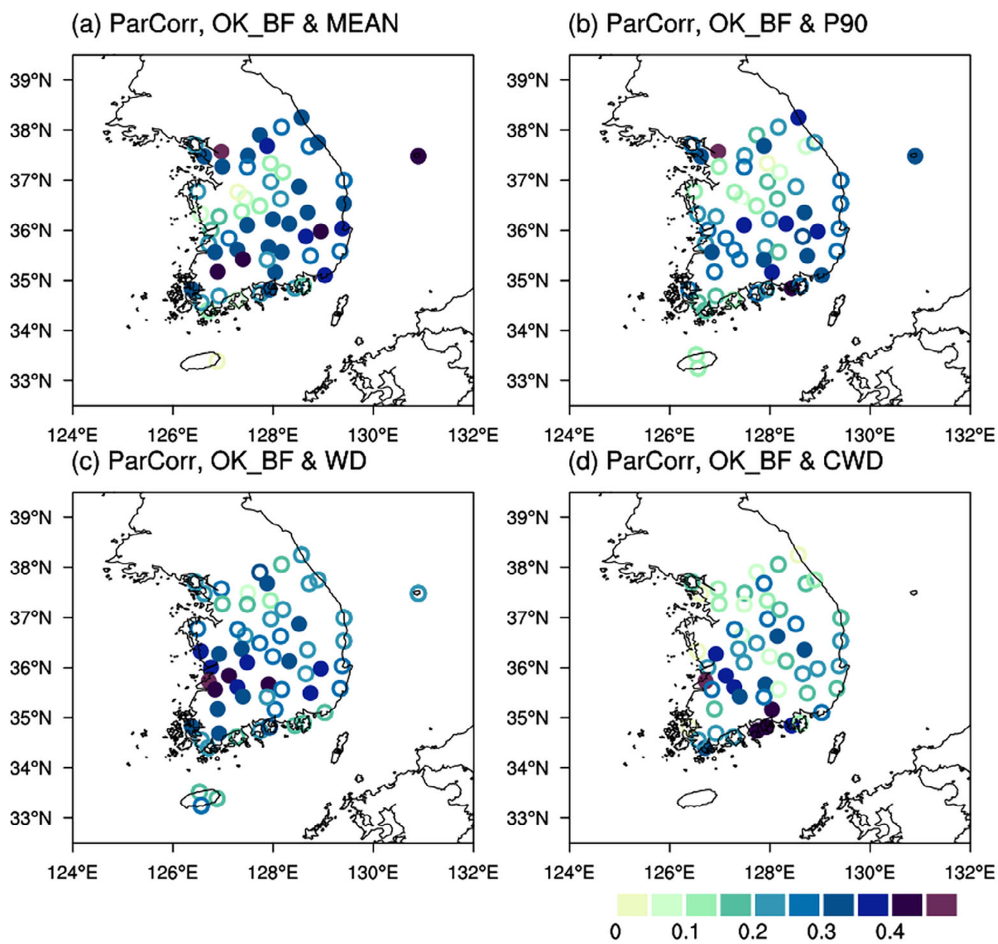


**FIGURE 11** Partial correlation maps between OK_BF and (a) MEAN, (b) P90, (c) WD, and (d) CWD after excluding the effects of the LLMW. The closed circles indicate that the correlation coefficients are significant at the 95% confidence level [Colour figure can be viewed at wileyonlinelibrary.com]

blocking appearance. These results show that the frequent occurrence of OKB can increase baroclinic instability over South Korea, resulting in cyclonic circulations and increased precipitation over the same regions.

Figure 11 presents partial correlation coefficients between OK_BF and precipitation indices after excluding the effects of the LLMW. This study analysed several statistical measures of daily precipitation, such as the mean precipitation (MEAN), extreme precipitation intensity (P90), wet days (WD), and consecutive wet days (CWD). The averaged intensity of the upper-10th percentile daily precipitation per year, P90, was considered. The WD was defined as daily precipitation higher than 1.0 mm, and the CWD was defined as a maximum number of consecutive wet days during summer. The OK_BF was closely related to the variability of the wet days and extreme precipitation as well as mean precipitation over most regions in South Korea (Figure 11). Regarding the mean and extreme precipitation, significant correlations with the OK_BF were found over the northern regions, eastern coastal regions, and southern regions in South Korea (Figures 11a-b). As Park and Ahn (2014) mentioned, the insignificant correlations in the central regions are due mainly to characteristics of regional precipitation. The Taebaek Mountains with high topography (mostly above 1,000 m) are located along the eastern coastal regions in South Korea (Figure 1a). Therefore, precipitation may decrease in the regions located on the leeward side of the mountains because of the effects of Fohn-type winds (easterly wind) induced by the OKB (Figure 12). With wet days, significant values were obtained over the entire regions in South Korea without regional characteristics (Figures 11c-d). The partial correlation coefficients between OK_BF and area-averaged MEAN, P90, WD, and CWD were 0.40, 0.37, 0.35, and 0.37, respectively, which are significant at the 95% confidence level (Table 2). Despite the characteristics of regional precipitation in South Korea, the frequent occurrence of OKB is closely associated with precipitation in South Korea over interannual timescales. These findings suggest that the Korean summer precipitation also can be modulated by baroclinic instability in association with the OK_BF, regardless of the LLMW.

Although drought is strongly associated with the variability of precipitation, it can also be modulated by the temperature variation. Based on previous analysis, the dominant effects of the increasing OK_BF on climate

**TABLE 2** Partial correlation coefficients among the precipitation indices and OK_BF after excluding the effects of the LLMW for the period 1979–2020 (JJA)

| MEAN | P90 | WD | CWD |
|---|---|---|---|
| **0.40**[a] (47%) | **0.37**[b] (25%) | **0.35**[b] (32%) | **0.37**[b] (22%) |

*Note*: The bold values indicate the correlations between the area-averaged precipitation indices and OK_BF. The values in brackets "()" are the ratio of the stations where the correlations are significant at the 95% confidence level.
[a]Significant at the 99% confidence level.
[b]Significant at the 95% confidence level.

**TABLE 3** Same as Table 2, except for PET and P minus PET (P-PET)

| PET | P minus PET |
|---|---|
| **−0.39**[a] (85%) | **0.41**[a] (50%) |

[a]Significant at the 99% confidence level.

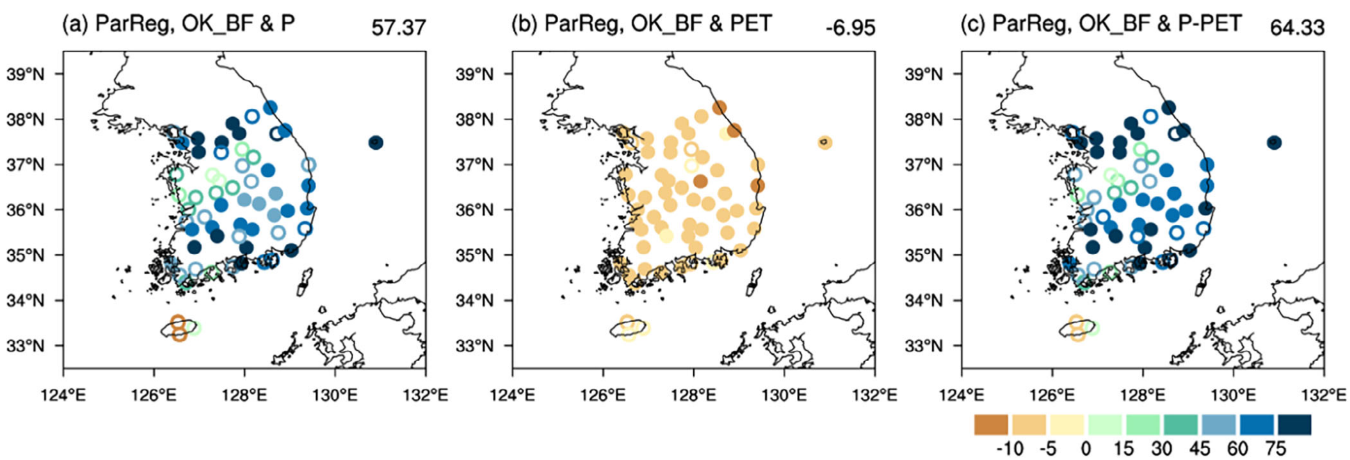


**FIGURE 13** Partial regression maps of three-month (June to august) accumulated (a) precipitation (P; unit: mm), (b) PET (unit: mm), and (c) P minus PET (unit: mm) onto the normalized OK_BF after excluding the effects of the LLMW. The closed circles indicate that the correlation coefficients are significant at the 95% confidence level. The value of the upper-right corner above each plot indicates the area-averaged value [Colour figure can be viewed at wileyonlinelibrary.com]

over South Korea are decreasing temperature and increasing precipitation. Thus, the change in the water budget can be attributed to the change in the OK_BF. Figure 13 shows the partial regression maps of the 3-month (June to August) accumulated precipitation (P), PET, and difference between precipitation and PET (P-PET), excluding the effects of the LLMW. The spatial patterns of accumulated precipitation were the same as those in Figure 11a (Figure 13a). A decrease in PET was observed over most regions in South Korea due to cold air advection under the influence of the increasing OK_BF (Figure 13b). Both increases in precipitation and decreases in PET helped intensify the hydrological water budget (Figure 13c). The partial correlation coefficients between OK_BF and area-averaged PET and P-PET were −0.39 and 0.41, respectively, which were significant at the 99% confidence level (Table 3). These results suggest that the effects of the increasing OK_BF on both precipitation and PET can reduce the drought risk over South Korea.

## 4 | DISCUSSION

As mentioned in the introduction, the formation of the OKH is related to the AEA teleconnection pattern or the PJ (or EAP) teleconnection pattern. In this section, this study investigated the evolution of OKB through composite analysis. Before applying the case composite analysis, we first defined OKB day if blocked longitudes are found at least five grid points (12.5°) in the Okhotsk Sea (140°E–160°E) on a certain day. One OKB event was defined if the OKB day lasts at least 5 days. In total, 28 OKB events were identified (Table 4). The following composite analyses were based on these identified 28 OKB events. For convenience, day 0 indicated the start date of OKB events and day $-n$ (day $+n$) represented the $n$th day before (after) the start date of OKB events. In addition, the horizontal wave activity flux (WAF) described by Takaya and Nakamura (2001) was calculated to represent the propagation of quasi-stationary Rossby waves.

Figure 14 represents the temporal variation of OKB events in the middle troposphere (500 hPa). On day −6, the eastward WAFs were detected from the North Atlantic to the Ural Mountains. From day −4 to day 0, the positive geopotential height anomalies near the Ural Mountains continued to be maintained and grew in magnitude. The eastward WAFs from Ural Mountains ramified into two branches. One propagated southeastward to Baikal Lake towards the middle latitudes, and the other propagated northeastward to Siberia towards the high latitudes. The persistent convergence between eastward WAFs from Siberia and northeastward WAFs from Baikal Lake further enhanced the OKH. These eastward WAFs resembled the AEA teleconnection pattern. Consequently, the double-blocking high pattern with the development of two blocking highs near the Ural Mountains and the Okhotsk Sea was predominantly characterized. Meanwhile, after day −2, the western extension of WNPSH (the positions of the 5,880 m isoline), which results in the growth of poleward WAFs from the tropics, was also identified, which was resembled the PJ or EAP teleconnection pattern. After day 0, the OKB became well-established and remained for at least 5 days, which maintained and reinforced the mid-latitude trough over NEA. These results suggested that the evolution of the OKB event was identified as having a more significant relationship with the eastward wave propagation at high latitudes than poleward energy propagation at low latitudes represented by the WAF.

Nevertheless, the impact of OKB events on precipitation over South Korea also should be considered in the individual blocking characteristics, such as duration, intensity, and extension. In addition, the relationship between the OKB events and summer precipitation over South Korea should be examined carefully over intra-seasonal timescales. The precipitation events are controlled mainly by other factors, such as the onset/peak/withdrawal period of BCM front and typhoon activities. According to a recent study, the occurrence of blocking in high latitudes led to stopping the northward march of the BCM front, leading to record-breaking BCM rainfall in June–July 2020 (Chen *et al.*, 2021). This suggests that further studies are needed to investigate the combined influence of the OKB and BCM front activities on precipitation over South Korea.

## 5 | SUMMARY

More than half of the annual precipitation in South Korea occurs in summer (JJA). Therefore, insufficient precipitation during that period can be related directly to the occurrence of droughts. Thus, understanding the variation in water resources is important for research related to drought and flood. OK_BF has a distinct negative (positive) correlation with the summer temperature (precipitation) in East Asia (Park and Ahn, 2014). These results suggest that OK_BF may influence the water budget components, including precipitation and PET, over South Korea. This study examined the detailed relationship between the OK_BF and both precipitation and PET over South Korea during summer using partial correlation and regression analyses.

Composite analysis for high and low PREC_SK years showed that the BFs over the Okhotsk Sea, particularly

**TABLE 4** Year, start date, end date, and duration (days) of the 28 OKB events

| Year | Start date (day month) | End date (day month) | Duration (days) |
|---|---|---|---|
| 1981 | 24 June | 04 July | 11 |
| 1983 | 08 June | 12 June | 5 |
| 1986 | 27 June | 01 July | 5 |
| 1986 | 14 June | 19 June | 6 |
| 1989 | 06 June | 17 June | 12 |
| 1990 | 08 July | 12 July | 5 |
| 1992 | 28 July | 02 August | 6 |
| 1993 | 16 July | 21 July | 6 |
| 1993 | 24 June | 29 June | 6 |
| 1995 | 21 June | 26 June | 6 |
| 1996 | 19 June | 24 June | 6 |
| 1998 | 04 June | 09 June | 6 |
| 1998 | 17 June | 21 June | 5 |
| 2000 | 16 July | 20 July | 5 |
| 2001 | 24 July | 01 August | 9 |
| 2002 | 18 June | 26 June | 9 |
| 2003 | 31 July | 06 August | 7 |
| 2003 | 19 July | 25 July | 7 |
| 2006 | 04 June | 10 June | 7 |
| 2006 | 12 July | 16 July | 5 |
| 2008 | 16 July | 21 July | 6 |
| 2009 | 10 June | 20 June | 11 |
| 2011 | 28 July | 01 August | 5 |
| 2012 | 09 July | 15 July | 7 |
| 2014 | 24 August | 28 August | 5 |
| 2015 | 24 June | 02 July | 9 |
| 2016 | 2 June | 08 June | 7 |
| 2020 | 15 June | 23 June | 9 |

in the regions of 140°E–160°E, were closely related to the precipitation over South Korea. Thus, this study defined the OK_BF as the area-averaged BFs over the region and examined the relationship between PREC_SK and OK_BF.

Although the correlation coefficient between OK_BF and PREC_SK was 0.27, which is not significant at the 95% confidence level, significant positive correlations were observed at some stations (10 stations) over South Korea. Park and Ahn (2014) attributed this insignificant relationship to the locality of precipitation. Nevertheless, it is still unclear if this relationship is robust and how OK_BF contributes to precipitation variability.

This study performed partial correlation and regression analyses to separate the contribution of the OK_BF to precipitation variability from that of the LLMW. The low-level warm and moist air advection over South Korea strongly modulates the precipitation variability over that region. The correlation coefficient between LLMW and PREC_SK was 0.51, which is significant at the 99% confidence level. The correlation coefficient between the OK_BF and LLMW was −0.13, suggesting that both variations are statistically independent. The partial correlation coefficient between OK_BF and PREC_SK after excluding the effects of the LLMW was 0.40, which is significant at the 99% confidence level. Furthermore, significant positive correlations were observed at most stations (28 stations) over South Korea. The analysis suggests that the variability of PREC_SK can also be modulated by the change in OK_BF, regardless of the change in low-level air advection from low latitudes. Thus, these statistical methods might be even more suitable for examining the impacts of OK_BF on precipitation.

The vertical structures of positive geopotential height anomalies associated with the increasing OK_BF can

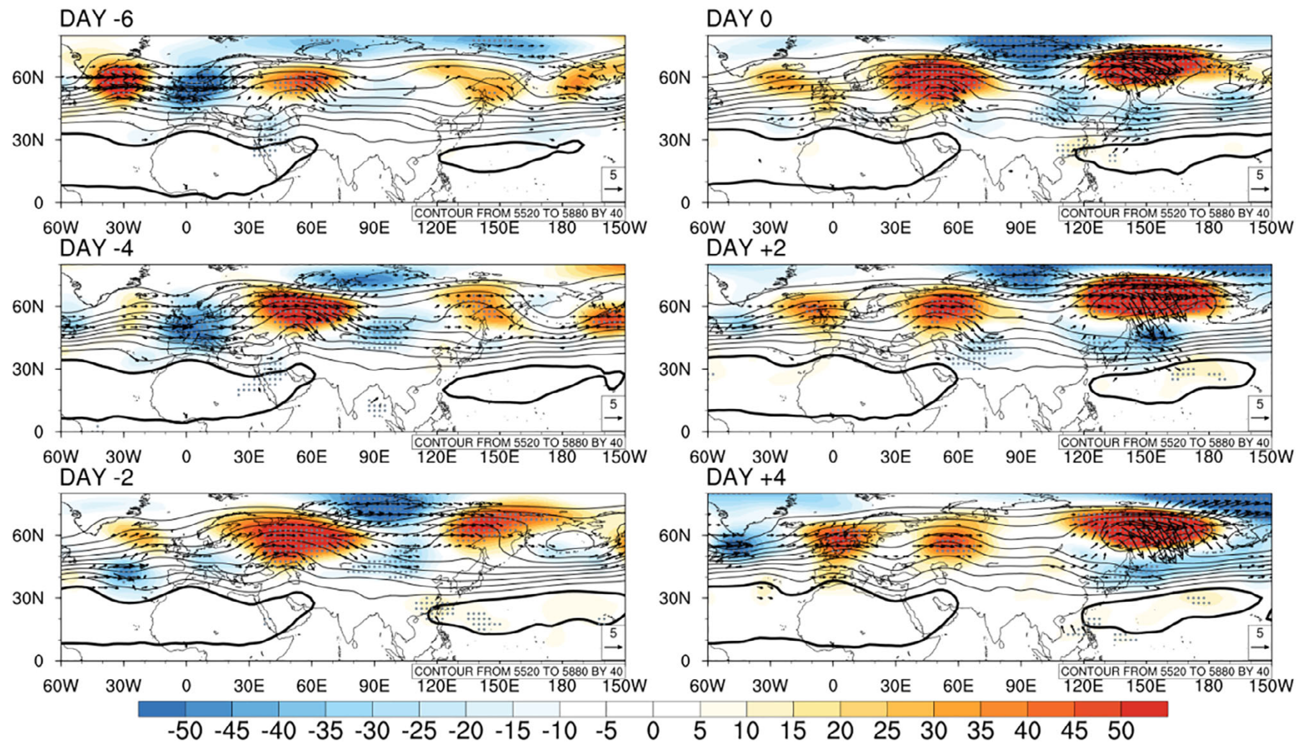


FIGURE 14 Composite of geopotential (shading; unit: m) and WAF (vector; unit: $m^2 \cdot s^{-2}$) anomalies at 500 hPa. The grey dots indicate that the anomalies are significant at the 95% confidence level. WAF anomalies less than 1.0 $m^2 \cdot s^{-2}$ in both directions are omitted. The values at the top-left corner above each plot indicate the days leading (negative) and lagging (positive) the onset of OKB events. The contours (thick contours) represent the composite geopotential height (5,880 m) at 500 hPa [Colour figure can be viewed at wileyonlinelibrary.com]

induce an enhanced meridional temperature gradient over South Korea caused by the equatorward advection of cold air masses from higher latitudes. The enhanced meridional temperature gradient can induce baroclinic instability, resulting in increased precipitation over the region. These results suggest that Korean summer precipitation can also be modulated by the baroclinic instability associated with the OK_BF, regardless of the LLMW.

The OK_BF was closely related to the variability of precipitation indices, including mean precipitation, extreme precipitation intensity, wet days, and consecutive wet days, over most regions in South Korea. In addition, the dominant effects of the increasing OK_BF on climate over South Korea are the decreasing PET and increasing precipitation. These results suggest that water resources may be abundant when OKB occurs frequently.

## ACKNOWLEDGEMENTS

We wish to thank four anonymous reviewers for their comments and suggestions, which helped improve the quality of this paper. This work was funded by the Korea Meteorological Administration Research and Development Program under Grant No. KMI2020-01411. The CMAP precipitation reanalysis data were downloaded from https://psl.noaa.gov/data/gridded/data.cmap.html. The NCEP2 reanalysis data were downloaded from https://psl.noaa.gov/data/gridded/data.ncep.reanalysis2.html. The weather station data over South Korea provided by Korean Meteorological Administration could be found in https://data.kma.go.kr. The ASTGTM3 data were obtained from https://search.earthdata.nasa.gov/search?q=C1711961296-LPCLOUD.

## AUTHOR CONTRIBUTIONS

**Chan-Yeong Song:** Formal analysis; investigation; methodology; visualization; writing – original draft. **Joong-Bae Ahn:** Conceptualization; supervision; validation; writing – review and editing.

## ORCID

*Chan-Yeong Song* https://orcid.org/0000-0002-8444-3938
*Joong-Bae Ahn* https://orcid.org/0000-0001-6958-2801

## REFERENCES

Abrams, M., Crippen, R. and Fujisada, H. (2020) ASTER global digital elevation model (GDEM) and ASTER global water body dataset (ASTWBD). *Remote Sensing*, 12(7), 1156. https://doi.org/10.3390/rs12071156.

Antokhina, O.Y., Antokhin, P., Martynova, Y. and Mordvinov, V. (2016) The impact of atmospheric blocking on spatial distributions of summertime precipitation over Eurasia. *IOP Conference Series: Earth and Environmental Science*, 48, 012035. https://doi.org/10.1088/1755-1315/48/1/012035.

Arai, M. and Kimoto, M. (2005) Relationship between springtime surface temperature and early summer blocking activity over Siberia. *Journal of the Meteorological Society of Japan*, 83(2), 261–267. https://doi.org/10.2151/jmsj.83.261.

As-syakur, A.R., Adnyana, I.W.S., Mahendra, M.S., Arthana, I.W., Merit, I.N., Kasa, I.W., Ekayanti, N.W., Nuarsa, I.W. and Sunarta, I.N. (2014) Observation of spatial patterns on the rainfall response to ENSO and IOD over Indonesia using TRMM multisatellite precipitation analysis (TMPA). *International Journal of Climatology*, 34(15), 3825–3839. https://doi.org/10.1002/joc.3939.

Azam, M., Maeng, S.-J., Kim, H.-S., Lee, S.-W. and Lee, J.-E. (2018) Spatial and temporal trend analysis of precipitation and drought in South Korea. *Water*, 10(6), 765. https://doi.org/10.3390/w10060765.

Baek, H.-J., Kim, M.-K. and Kwon, W.-T. (2017) Observed short- and long-term changes in summer precipitation over South Korea and their links to large-scale circulation anomalies. *International Journal of Climatology*, 37(2), 972–986. https://doi.org/10.1002/joc.4753.

Barriopedro, D., García-Herrera, R., Lupo, A.R. and Hernández, E. (2006) A climatology of northern hemisphere blocking. *Journal of Climate*, 19(6), 1042–1063. https://doi.org/10.1175/jcli3678.1.

Barriopedro, D., Fischer, E.M., Luterbacher, J., Trigo, R.M. and García-Herrera, R. (2011) The hot summer of 2010: redrawing the temperature record map of Europe. *Science*, 332(6026), 220–224. https://doi.org/10.1126/science.1201224.

Buehler, T., Raible, C.C. and Stocker, T.F. (2011) The relationship of winter season North Atlantic blocking frequencies to extreme cold or dry spells in the ERA-40. *Tellus A: Dynamic Meteorology and Oceanography*, 63(2), 212–222. https://doi.org/10.1111/j.1600-0870.2010.00492.x.

Chang, C.-P., Zhang, Y. and Li, T. (2000a) Interannual and interdecadal variations of the east Asian summer monsoon and tropical Pacific SSTs. Part I: roles of the subtropical ridge. *Journal of Climate*, 13(24), 4310–4325. https://doi.org/10.1175/1520-0442(2000)013<4310:Iaivot>2.0.Co;2.

Chang, C.-P., Zhang, Y. and Li, T. (2000b) Interannual and interdecadal variations of the east Asian summer monsoon and tropical Pacific SSTs. Part II: meridional structure of the monsoon. *Journal of Climate*, 13(24), 4326–4340. https://doi.org/10.1175/1520-0442(2000)013<4326:Iaivot>2.0.Co;2.

Chen, X., Dai, A., Wen, Z. and Song, Y. (2021) Contributions of Arctic Sea-ice loss and east Siberian atmospheric blocking to 2020 record-breaking Meiyu-Baiu rainfall. *Geophysical Research Letters*, 48(10), e2021GL092748. https://doi.org/10.1029/2021GL092748.

Chen, Y. and Zhai, P. (2014a) Precursor circulation features for persistent extreme precipitation in central-eastern China. *Weather and Forecasting*, 29(2), 226–240. https://doi.org/10.1175/waf-d-13-00065.1.

Chen, Y. and Zhai, P. (2014b) Two types of typical circulation pattern for persistent extreme precipitation in Central–Eastern China. *Quarterly Journal of the Royal Meteorological Society*, 140(682), 1467–1478. https://doi.org/10.1002/qj.2231.

Chen, Y. and Zhai, P. (2015) Synoptic-scale precursors of the East Asia/Pacific teleconnection pattern responsible for persistent extreme precipitation in the Yangtze River Valley. *Quarterly Journal of the Royal Meteorological Society*, 141(689), 1389–1403. https://doi.org/10.1002/qj.2448.

Choi, K.-S., Kim, D.-W. and Byun, H.-R. (2009) Possible impact of spring sea ice anomaly in the North Pacific on the Korean summer drought. *Asia-Pacific Journal of Atmospheric Sciences*, 45(3), 331–346.

Choi, K.-S., Oh, S.-B., Byun, H.-R., Kripalani, R.H. and Kim, D.-W. (2011) Possible linkage between east Asian summer drought and North Pacific oscillation. *Theoretical and Applied Climatology*, 103(1), 81–93. https://doi.org/10.1007/s00704-010-0286-7.

Choi, Y.-W., Ahn, J.-B., Suh, M.-S., Cha, D.-H., Lee, D.-K., Hong, S.-Y., Min, S.-K., Park, S.-C. and Kang, H.-S. (2016) Future changes in drought characteristics over South Korea using multi regional climate models with the standardized precipitation index. *Asia-Pacific Journal of Atmospheric Sciences*, 52(2), 209–222. https://doi.org/10.1007/s13143-016-0020-1.

Choi, Y.-W. and Ahn, J.-B. (2017) The effect of boreal late autumn snow cover over Western and Central China on the northern hemisphere wintertime blocking frequency. *Journal of Climate*, 30(22), 9027–9039. https://doi.org/10.1175/jcli-d-16-0830.1.

Choi, Y.-W. and Ahn, J.-B. (2019) Possible mechanisms for the coupling between late spring sea surface temperature anomalies over tropical Atlantic and east Asian summer monsoon. *Climate Dynamics*, 53(11), 6995–7009. https://doi.org/10.1007/s00382-019-04970-3.

Eady, E.T. (1949) Long waves and cyclone waves. *Tellus*, 1(3), 33–52. https://doi.org/10.3402/tellusa.v1i3.8507.

Easterling, D.R., Wallis, T.W.R., Lawrimore, J.H. and Heim, R.R., Jr. (2007) Effects of temperature and precipitation trends on U.S. drought. *Geophysical Research Letters*, 34(20), L20709. https://doi.org/10.1029/2007GL031541.

Fernandes, L.G. and Rodrigues, R.R. (2018) Changes in the patterns of extreme rainfall events in southern Brazil. *International Journal of Climatology*, 38(3), 1337–1352. https://doi.org/10.1002/joc.5248.

García-Herrera, R., Hernández, E., Barriopedro, D., Paredes, D., Trigo, R.M., Trigo, I.F. and Mendes, M.A. (2007) The outstanding 2004/05 drought in the Iberian Peninsula: associated atmospheric circulation. *Journal of Hydrometeorology*, 8(3), 483–498. https://doi.org/10.1175/jhm578.1.

Gong, D.-Y. and Ho, C.-H. (2003) Arctic oscillation signals in the east Asian summer monsoon. *Journal of Geophysical Research—Atmospheres*, 108(D2), 4066. https://doi.org/10.1029/2002JD002193.

Gong, D.-Y., Yang, J., Kim, S.-J., Gao, Y., Guo, D., Zhou, T. and Hu, M. (2011) Spring Arctic oscillation-east Asian summer monsoon connection through circulation changes over the western North Pacific. *Climate Dynamics*, 37(11), 2199–2216. https://doi.org/10.1007/s00382-011-1041-1.

Grams, C.M., Binder, H., Pfahl, S., Piaget, N. and Wernli, H. (2014) Atmospheric processes triggering the central European floods in June 2013. *Natural Hazards and Earth System Sciences*, 14(7), 1691–1702. https://doi.org/10.5194/nhess-14-1691-2014NHESS.

Ha, K.-J., Park, S.-K. and Kim, K.-Y. (2003) Interannual variability in summer precipitation around the Korean peninsula and its associated east Asian summer circulation. *Atmosphere*, 39(5), 575–586 (in Korean with English abstract).

Ha, K.-J., Heo, K.-Y., Lee, S.-S., Yun, K.-S. and Jhun, J.-G. (2012) Variability in the east Asian monsoon: a review. *Meteorological Applications*, 19(2), 200–215. https://doi.org/10.1002/met.1320.

Ham, Y.-G., Chikamoto, Y., Kug, J.-S., Kimoto, M. and Mochizuki, T. (2017) Tropical Atlantic-Korea teleconnection pattern during boreal summer season. *Climate Dynamics*, 49(7), 2649–2664. https://doi.org/10.1007/s00382-016-3474-z.

He, J. and Zhu, Z. (2015) The relation of South China Sea monsoon onset with the subsequent rainfall over the subtropical East Asia. *International Journal of Climatology*, 35(15), 4547–4556. https://doi.org/10.1002/joc.4305.

He, Y., Huang, J., Li, D., Xie, Y., Zhang, G., Qi, Y., Wang, S. and Totz, S. (2018) Comparison of the effect of land-sea thermal contrast on interdecadal variations in winter and summer blockings. *Climate Dynamics*, 51(4), 1275–1294. https://doi.org/10.1007/s00382-017-3954-9.

Hong, J.-Y. and Ahn, J.-B. (2015) Changes of early summer precipitation in the Korean peninsula and nearby regions based on RCP simulations. *Journal of Climate*, 28(9), 3557–3578. https://doi.org/10.1175/jcli-d-14-00504.1.

Hoskins, B.J. and Valdes, P.J. (1990) On the existence of storm-tracks. *Journal of the Atmospheric Sciences*, 47(15), 1854–1864. https://doi.org/10.1175/1520-0469(1990)047<1854:Oteost>2.0.Co;2.

Hwang, S.-O. and Lee, D.-K. (1993) A study on the relationship between heavy rainfalls and associated low-level jets in the Korean peninsula. *Asia-Pacific Journal of Atmospheric Sciences*, 29(2), 133–146 (in Korean with English abstract).

Im, E.-S., Ahn, J.-B. and Kim, D.-W. (2012) An assessment of future dryness over Korea based on the ECHAM5-RegCM3 model chain under A1B emission scenario. *Asia-Pacific Journal of Atmospheric Sciences*, 48(4), 325–337. https://doi.org/10.1007/s13143-012-0031-5.

Kanamitsu, M., Ebisuzaki, W., Woollen, J., Yang, S.-K., Hnilo, J.J., Fiorino, M. and Potter, G.L. (2002) NCEP–DOE AMIP-II reanalysis (R-2). *Bulletin of the American Meteorological Society*, 83(11), 1631–1644. https://doi.org/10.1175/bams-83-11-1631.

Kim, B.-S., Sung, J.-H., Kang, H.-S. and Cho, C.-H. (2012) Assessment of drought severity over South Korea using standardized precipitation evapo-transpiration index (SPEI). *Journal of Korea Water Resources Association*, 45(9), 887–900. https://doi.org/10.3741/JKWRA.2012.45.9.887 (in Korean with English abstract).

Kim, B.-S., Sung, J.-H., Lee, B.-H. and Kim, D.-J. (2013) Evaluation on the impact of extreme droughts in South Korea using the SPEI and RCP8. 5 climate change scenario. *Journal of the Korean Society of Hazard Mitigation*, 13(2), 97–109. https://doi.org/10.9798/KOSHAM.2013.13.2.097 (in Korean with English abstract).

Kim, D.-W., Byun, H.-R., Choi, K.-S. and Oh, S.-B. (2011) A spatio-temporal analysis of historical droughts in Korea. *Journal of Applied Meteorology and Climatology*, 50(9), 1895–1912. https://doi.org/10.1175/2011jamc2664.1.

Kim, J.-Y., Seo, K.-H., Yeh, S.-W., Kim, H.-K., Yim, S.-Y., Lee, H.-S., Kown, M. and Ham, Y.-G. (2017) Analysis of characteristics for 2016 Changma rainfall. *Atmosphere*, 27(3), 277–290. https://doi.org/10.14191/Atmos.2017.27 (in Korean with English abstract).

Kim, S. and Kug, J.-S. (2018) What controls ENSO teleconnection to East Asia? Role of Western North Pacific precipitation in ENSO teleconnection to East Asia. *Journal of Geophysical Research – Atmospheres*, 123(18), 10406–10422. https://doi.org/10.1029/2018JD028935.

Kwon, H.-H., Lall, U. and Kim, S.-J. (2016) The unusual 2013–2015 drought in South Korea in the context of a multicentury precipitation record: inferences from a nonstationary, multivariate, Bayesian copula model. *Geophysical Research Letters*, 43(16), 8534–8544. https://doi.org/10.1002/2016GL070270.

Kwon, M., Kwon, H.-H. and Han, D. (2019) Spatio-temporal drought patterns of multiple drought indices based on precipitation and soil moisture: a case study in South Korea. *International Journal of Climatology*, 39(12), 4669–4687. https://doi.org/10.1002/joc.6094.

Lee, D.Y. and Ahn, J.-B. (2017) Future change in the frequency and intensity of wintertime North Pacific blocking in CMIP5 models. *International Journal of Climatology*, 37(5), 2765–2781. https://doi.org/10.1002/joc.4878.

Lee, E.-J., Jhun, J.-G. and Park, C.-K. (2005) Remote connection of the northeast Asian summer rainfall variation revealed by a newly defined monsoon index. *Journal of Climate*, 18(21), 4381–4393. https://doi.org/10.1175/jcli3545.1.

Lee, M.-H., Im, E.-S. and Bae, D.-H. (2019) A comparative assessment of climate change impacts on drought over Korea based on multiple climate projections and multiple drought indices. *Climate Dynamics*, 53(1), 389–404. https://doi.org/10.1007/s00382-018-4588-2.

Lee, S.-E. and Seo, K.-H. (2013) The development of a statistical forecast model for Changma. *Weather and Forecasting*, 28(6), 1304–1321. https://doi.org/10.1175/waf-d-13-00003.1.

Lindzen, R.S. and Farrell, B. (1980) A simple approximate result for the maximum growth rate of Baroclinic instabilities. *Journal of the Atmospheric Sciences*, 37(7), 1648–1654. https://doi.org/10.1175/1520-0469(1980)037<1648:Asarft>2.0.Co;2.

Mann, H.B. and Whitney, D.R. (1947) On a test of whether one of two random variables is stochastically larger than the other. *Annals of Mathematical Statistics*, 18(1), 50–60.

Min, S.-K., Kwon, W.-T., Park, E.-H. and Choi, Y. (2003) Spatial and temporal comparisons of droughts over Korea with East Asia. *International Journal of Climatology*, 23(2), 223–233. https://doi.org/10.1002/joc.872.

Mullen, S.L. (1987) Transient Eddy forcing of blocking flows. *Journal of the Atmospheric Sciences*, 44(1), 3–22. https://doi.org/10.1175/1520-0469(1987)044<0003:Tefobf>2.0.Co;2.

Nakamura, H. and Wallace, J.M. (1993) Synoptic behavior of baroclinic eddies during the blocking onset. *Monthly Weather Review*, 121(7), 1892–1903. https://doi.org/10.1175/1520-0493(1993)121<1892:Sbobed>2.0.Co;2.

Nakamura, H. and Fukamachi, T. (2004) Evolution and dynamics of summertime blocking over the Far East and the associated surface Okhotsk high. *Quarterly Journal of the Royal Meteorological Society*, 130(599), 1213–1233. https://doi.org/10.1256/qj.03.101.

Nam, W.-H., Hayes, M.J., Wilhite, D.A. and Svoboda, M.D. (2015) Projection of temporal trends on drought characteristics using the standardized precipitation evapotranspiration index (SPEI) in South Korea. *Journal of Korean Society of Agricultural*

*Engineers*, 57(1), 37–45. https://doi.org/10.5389/KSAE.2015.57.1.037 (in Korean with English abstract).

Ninomiya, K. and Mizuno, H. (1985) Anomalous cold spell in summer over northeastern Japan caused by northeasterly wind from polar maritime airmass part 1. EOF analysis of temperature variation in relation to the large-scale situation causing the cold summer. *Journal of the Meteorological Society of Japan*, 63(5), 845–857. https://doi.org/10.2151/jmsj1965.63.5_845.

Nitta, T. (1987) Convective activities in the tropical Western Pacific and their impact on the northern hemisphere summer circulation. *Journal of the Meteorological Society of Japan*, 65(3), 373–390. https://doi.org/10.2151/jmsj1965.65.3_373.

Ogi, M., Yamazaki, K. and Tachibana, Y. (2005) The summer northern annular mode and abnormal summer weather in 2003. *Geophysical Research Letters*, 32(4). L04706. https://doi.org/10.1029/2004GL021528.

Park, C.-H., Lee, H.-W. and Jung, W.-S. (2003) The effects of low-level jet and topography on heavy rainfall near Mt. Jirisan. *Atmosphere*, 39(4), 441–458 (in Korean with English abstract).

Park, H.-J., Kryjov, V.N. and Ahn, J.-B. (2018) One-month-lead predictability of Asian summer monsoon indices based on the zonal winds by the APCC multimodel ensemble. *Journal of Climate*, 31(21), 8945–8960. https://doi.org/10.1175/jcli-d-17-0816.1.

Park, H.-L., Seo, K.-H. and Son, J.-H. (2015) Development of a dynamics-based statistical prediction model for the Changma onset. *Journal of Climate*, 28(17), 6647–6666. https://doi.org/10.1175/jcli-d-14-00502.1.

Park, Y.-J. and Ahn, J.-B. (2014) Characteristics of atmospheric circulation over East Asia associated with summer blocking. *Journal of Geophysical Research—Atmospheres*, 119(2), 726–738. https://doi.org/10.1002/2013JD020688.

Rex, D.F. (1950a) Blocking action in the middle troposphere and its effect upon regional climate. *Tellus*, 2(3), 196–211. https://doi.org/10.3402/tellusa.v2i3.8546.

Rex, D.F. (1950b) Blocking action in the middle troposphere and its effect upon regional climate. *Tellus*, 2(4), 275–301. https://doi.org/10.3402/tellusa.v2i4.8603.

Rodrigues, R.R. and Woollings, T. (2017) Impact of atmospheric blocking on South America in Austral summer. *Journal of Climate*, 30(5), 1821–1837. https://doi.org/10.1175/jcli-d-16-0493.1.

Shin, C.-S. and Lee, T.-Y. (2005) Development mechanisms for the heavy rainfalls of 6–7 August 2002 over the middle of the Korean peninsula. *Journal of the Meteorological Society of Japan*, 83(5), 683–709. https://doi.org/10.2151/jmsj.83.683.

Shutts, G.J. (1983) The propagation of eddies in diffluent jetstreams: Eddy vorticity forcing of 'blocking' flow fields. *Quarterly Journal of the Royal Meteorological Society*, 109(462), 737–761. https://doi.org/10.1002/qj.49710946204.

Sohn, S.-J., Ahn, J.-B. and Tam, C.-Y. (2013) Six month–lead downscaling prediction of winter to spring drought in South Korea based on a multimodel ensemble. *Geophysical Research Letters*, 40(3), 579–583. https://doi.org/10.1002/grl.50133.

Sousa, P.M., Barriopedro, D., Trigo, R.M., Ramos, A.M., Nieto, R., Gimeno, L., Turkman, K.F. and Liberato, M.L.R. (2016) Impact of Euro-Atlantic blocking patterns in Iberia precipitation using a novel high resolution dataset. *Climate Dynamics*, 46(7), 2573–2591. https://doi.org/10.1007/s00382-015-2718-7.

Sousa, P.M., Trigo, R.M., Barriopedro, D., Soares, P.M.M., Ramos, A.M. and Liberato, M.L.R. (2017) Responses of European precipitation distributions and regimes to different blocking locations. *Climate Dynamics*, 48(3), 1141–1160. https://doi.org/10.1007/s00382-016-3132-5.

Tachibana, Y., Nakamura, T., Komiya, H. and Takahashi, M. (2010) Abrupt evolution of the summer northern hemisphere annular mode and its association with blocking. *Journal of Geophysical Research—Atmospheres*, 115(D12), D12125. https://doi.org/10.1029/2009JD012894.

Takaya, K. and Nakamura, H. (2001) A formulation of a phase-independent wave-activity flux for stationary and migratory quasigeostrophic eddies on a zonally varying basic flow. *Journal of the Atmospheric Sciences*, 58(6), 608–627. https://doi.org/10.1175/1520-0469(2001)058<0608:Afoapi>2.0.Co;2.

Thornthwaite, C.W. (1948) An approach toward a rational classification of climate. *Geographical Review*, 38(1), 55–94. https://doi.org/10.2307/210739.

Tibaldi, S. and Molteni, F. (1990) On the operational predictability of blocking. *Tellus A*, 42(3), 343–365. https://doi.org/10.1034/j.1600-0870.1990.t01-2-00003.x.

Vicente-Serrano, S.M., Beguería, S. and López-Moreno, J.I. (2010) A multiscalar drought index sensitive to global warming: the standardized precipitation evapotranspiration index. *Journal of Climate*, 23(7), 1696–1718. https://doi.org/10.1175/2009jcli2909.1.

Wang, B., Wu, R. and Fu, X. (2000) Pacific-east Asian teleconnection: how does ENSO affect east Asian climate? *Journal of Climate*, 13(9), 1517–1536. https://doi.org/10.1175/1520-0442(2000)013<1517:Peathd>2.0.Co;2.

Wang, B., Wu, Z., Li, J., Liu, J., Chang, C.-P., Ding, Y. and Wu, G. (2008) How to measure the strength of the east Asian summer monsoon. *Journal of Climate*, 21(17), 4449–4463. https://doi.org/10.1175/2008jcli2183.1.

Wang, L., Wang, C. and Guo, D. (2018) Evolution mechanism of synoptic-scale EAP teleconnection pattern and its relationship to summer precipitation in China. *Atmospheric Research*, 214, 150–162. https://doi.org/10.1016/j.atmosres.2018.07.023.

Wang, Y. (1992) Effects of blocking anticyclones in Eurasia in the rainy season (Meiyu/Baiu season). *Journal of the Meteorological Society of Japan*, 70(5), 929–951. https://doi.org/10.2151/jmsj1965.70.5_929.

Wu, Z., Wang, B., Li, J. and Jin, F.-F. (2009) An empirical seasonal prediction model of the east Asian summer monsoon using ENSO and NAO. *Journal of Geophysical Research—Atmospheres*, 114(D18), D18120. https://doi.org/10.1029/2009JD011733.

Wu, Z., Li, J., Jiang, Z., He, J. and Zhu, X. (2012) Possible effects of the North Atlantic oscillation on the strengthening relationship between the east Asian summer monsoon and ENSO. *International Journal of Climatology*, 32(5), 794–800. https://doi.org/10.1002/joc.2309.

Xie, P. and Arkin, P.A. (1997) Global precipitation: a 17-year monthly analysis based on gauge observations, satellite estimates, and numerical model outputs. *Bulletin of the American Meteorological Society*, 78(11), 2539–2558. https://doi.org/10.1175/1520-0477(1997)078<2539:Gpayma>2.0.Co;2.

Yeo, S.-R., Kwon, M. and Lee, J.-Y. (2020) The non-linear relationship between the western North Pacific anticyclonic circulation and Korean summer precipitation on subseasonal timescales.

*Climate Dynamics*, 54(1), 525–541. https://doi.org/10.1007/s00382-019-05013-7.

Yim, S.-Y., Yeh, S.-W., Wu, R. and Jhun, J.-G. (2008) The influence of ENSO on decadal variations in the relationship between the east Asian and Western North Pacific summer monsoons. *Journal of Climate*, 21(13), 3165–3179. https://doi.org/10.1175/2007jcli1948.1.

You, J.-E. and Ahn, J.-B. (2012) The anomalous structures of atmospheric and oceanic variables associated with the frequency of North Pacific winter blocking. *Journal of Geophysical Research – Atmospheres*, 117(D11), D11108. https://doi.org/10.1029/2012JD017431.

Yun, K.-S., Ha, K.-J. and Wang, B. (2010) Impacts of tropical ocean warming on east Asian summer climate. *Geophysical Research Letters*, 37(20), L20809. https://doi.org/10.1029/2010GL044931.

Zhang, L. and Zhou, T. (2015) Drought over East Asia: a review. *Journal of Climate*, 28(8), 3375–3399. https://doi.org/10.1175/jcli-d-14-00259.1.

Zheng, F., Li, J., Li, Y., Zhao, S. and Deng, D. (2016) Influence of the summer NAO on the spring-NAO-based predictability of the east Asian summer monsoon. *Journal of Applied Meteorology and Climatology*, 55(7), 1459–1476. https://doi.org/10.1175/jamc-d-15-0199.1.

Zuo, J.-Q., Li, W.-J., Ren, H.-L. and Chen, L.-J. (2012) Change of the relationship between the spring NAO and east Asian summer monsoon and its possible mechanism. *Chinese Journal of Geophysics*, 55(1), 23–34. https://doi.org/10.1002/cjg2.1697.

Zuo, J.-Q., Li, W., Sun, C., Xu, L. and Ren, H.-L. (2013) Impact of the North Atlantic Sea surface temperature tripole on the east Asian summer monsoon. *Advances in Atmospheric Sciences*, 30(4), 1173–1186. https://doi.org/10.1007/s00376-012-2125-5.

## SUPPORTING INFORMATION

Additional supporting information may be found in the online version of the article at the publisher's website.

**How to cite this article:** Song, C.-Y., & Ahn, J.-B. (2021). Influence of Okhotsk Sea blocking on summer precipitation over South Korea. *International Journal of Climatology*, 1–18. https://doi.org/10.1002/joc.7432